9

Phase Transitions in Layered Semiconductor - Ferroelectrics

Andrius Dziaugys[1], Juras Banys[1], Vytautas Samulionis[1], Jan Macutkevic[2], Yulian Vysochanskii[3], Vladimir Shvartsman[4] and Wolfgang Kleemann[5]
[1]*Department of Radiophysics, Faculty of Physics, Vilnius University, 2600 Vilnius*
[2]*Center for Physical Sciences and Technology, A. Gostauto 11, 2600 Vilnius*
[3]*Institute of Solid State Physics and Chemistry, Uzhgorod University, Uzhgorod 88000*
[4]*Institute for Materials Science, Duisburg-Essen University, 45141 Essen*
[5]*Faculty of physics, Duisburg-Essen University, 47048 Duisburg*
[1,2]*Lithuania*
[3]*Ukraine*
[4,5]*Germany*

1. Introduction

$CuInP_2S_6$ crystals represent an unusual example of an anticollinear uncompensated two-sublattice ferroelectric system (Maisonneuve et al., 1997). They exhibit a first-order phase transition of the order–disorder type from the paraelectric to the ferrielectric phase (T_c = 315 K). The symmetry reduction at the phase transition (C2/c to Cc) occurs due to the ordering in the copper sublattice and the displacement of cations from the centrosymmetric positions in the indium sublattice. X-ray investigations have shown that Cu ion can occupy three types of positions (Maisonneuve et al., 1997). The ordering of the Cu ions (hopping between Cu^1u and Cu^1d positions) in the double minimum potential is the reason for the phase transition dynamics in $CuInP_2S_6$. In (Maisonneuve et al., 1997) it was suggested that a coupling between P_2S_6 deformation modes and Cu^+ vibrations enable the copper ion hopping motions that lead to the onset of ionic conductivity in this material at higher temperatures. At low temperatures a dipolar glass phase appears in $CuInP_2S_6$ weakly doped with antiferroelectric $CuCrP_2S_6$ or ferroelectric $CuInP_2Se_6$ (Macutkevic et al., 2008).
The copper chromium thiophosphate $CuCrP_2S_6$ crystallizes in a layered two-dimensional structure of the $Cu^IM^{III}P_2S_6$ (M = Cr, In) type described above (Maisonneuve et al., 1995). It is formed by double sheets of sulfur atoms sandwiching the metal cations and P–P groups which occupy the octahedral voids defined by the sulfur atoms. At room temperature the crystal structure has a space group of C2/c (Colombet et al., 1982). At 64 K, the Cu positions are confined to those of an antiferroelectric order where the crystal structure has the space group of Pc (Maisonneuve et al., 1995). Thus, the mechanism of the dielectric transition is likely to involve hopping of the copper ions among two or more positions. Two phase transitions have been observed at 155 K and 190 K by dielectric measurement and differential scanning calorimetry (DSC). The crystal is antiferroelectric below 155 K and paraelectric above 190 K. For the intermediate phase between 155 and 190 K, a quasi-

antipolar structure has been proposed. Solid solutions $CuCr_{1-x}In_xP_2S_6$, $x > 0$, are therefore expected to reveal disordered dipolar glass phases as a consequence of randomness and frustration as confirmed recently (Maior et al., 2008).

Similar signatures of disorder might also be expected for the magnetic ground state of $CuCr_{1-x}In_xP_2S_6$, where magnetic Cr^{3+} ions are randomly replaced by diamagnetic In^{3+} ions in the antiferromagnetic (AF) compound $CuCrP_2S_6$ with a Néel temperature $T_N \approx 32$ K (Colombet et al., 1982). Owing to its competing ferromagnetic (FM) intralayer and AF interlayer exchange interactions (Colombet et al., 1982), randomness and frustration might eventually give rise to spin glass phases in $CuCr_{1-x}In_xP_2S_6$, $x > 0$, similarly as in the related AF compound $Fe_{1-x}Mg_xCl_2$ (Bertrand et al., 1982; Mattsson et al., 1996). The possible coexistence of this spin glass phase with the dipolar glassy one (Maior et al., 2008) is another timely motivation to study $CuCr_{1-x}In_xP_2S_6$. Indeed, '*multiglass*' behavior was recently discovered in the dilute magnetic perovskite $Sr_{0.98}Mn_{0.02}TiO_3$ (Shvartsman et al., 2008), paving the way to a new class of materials, '*disordered multiferroics*' (Kleemann et al., 2009).

The above mentioned comparison of the two families of dilute antiferromagnets $CuCrP_2S_6$:In and $FeCl_2$:Mg is not fortuitous. Originally, a strong structural analogy had been noticed between the lamellar compounds FeX_2 (X = Cl or Br) and transition metal (M) thio-phosphate phases, MPS_3, such as $FePS_3$ (Colombet et al., 1982). Both families are characterized by van der Waals gaps between their crystalline slabs and their ability to act as intercalation host material. The analogy becomes formally apparent when using the notations $Fe_2P_2S_6$ or – stressing the occurrence of P_2 pairs – $[Fe_{2/3}(P_2)_{1/3}]S_2$ (Klingen et al., 1973), and substituting $(Fe^{2+})_2$ by (Cu^+Cr^{3+}). This transcription discloses, however, that in contrast to the FeX_2 compounds even the undoped $CuCrP_2S_6$ is a 'dilute magnet' from the beginning (*i.e.* in the absence of non-magnetic In^{3+}), since it always hosts two diamagnetic cation sublattices occupied by Cu and P ions. This 'extra' dilution must be taken into account for understanding the magnetic and magnetoelectric properties discussed below.

This manuscript includes broad band spectroscopy, SQUID and piezoelectric measurement techniques, which helped to complement the list of already known properties of the investigated crystals and reveal new features such as dipole glass behaviour, magneto-electric coupling, and piezoelectric response. This crystal family is very interesting for various transducers because of the quite broad temperature region (285 to 330 K) for the phase transition.

2. Broad band dielectric spectroscopy of layered crystals

2.1 Ferrielectric phase transition in $CuInP_2S_6$, $Ag_{0.1}Cu_{0.9}InP_2S_6$ and $CuIn_{1+\delta}P_2S_6$ crystals

Results of the broadband dielectric measurements of $Ag_{0.1}Cu_{0.9}InP_2S_6$ are presented in Fig. 1. At low frequencies the dielectric losses increase with increasing temperature mainly due to the high ionic conductivity. The real part of the dielectric permittivity at 1 MHz already corresponds to the static one, because at that frequency ε'' is already much smaller than ε' (A. Dziaugys et al., 2010). It was found, that impurity of Ag ions, or addition of extra In ions drastically changes the ferrielectric phase transition temperature (static dielectric permittivity maximum temperature) (Table 1).

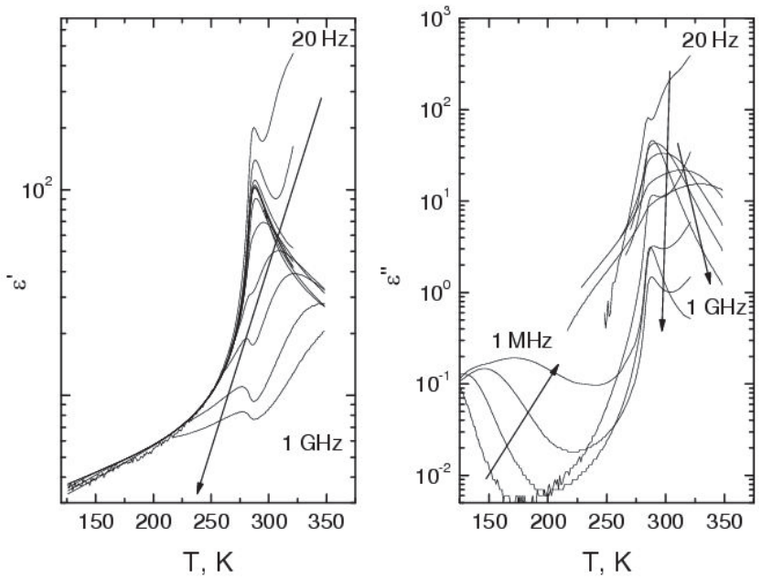

Fig. 1. Temperature dependence of the complex dielectric permittivity of $Ag_{0.1}Cu_{0.9}InP_2S_6$.

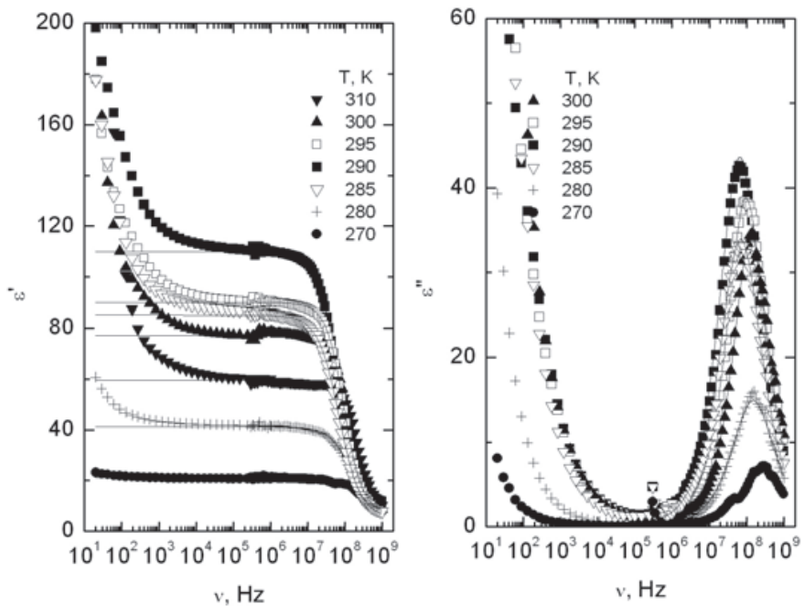

Fig. 2. Frequency dependence of complex dielectric permittivity of $Ag_{0.1}Cu_{0.9}InP_2S_6$ crystals measured at different temperatures. Solid lines are best fits according to *Eq.* (1).

Crystal	Phase transition temperature, K
$CuInP_2S_6$	313 (A. Dziaugys et al. 2010)
$CuIn_{1+\delta}P_2S_6$	330 (A. Dziaugys et al. 2011)
$Ag_{0.1}Cu_{0.9}InP_2S_6$	285 (A. Dziaugys et al. 2010)

Table 1. Phase transition temperatures got from the dielectric measurements.

The nature of such phase transition, similar to the pure $CuInP_2S_6$, is ferrielectric - ordering in the copper sublattice and displacement of cations from the centrosymmetric positions in the indium sublattice. The ferrielectric dispersion in the vicinity of T_c begins at about 10 MHz for $Ag_{0.1}Cu_{0.9}InP_2S_6$ and ranges up to the GHz region (Fig. 2). The characteristic minimum of ε' appears above 100 MHz at T = 285 K for $Ag_{0.1}Cu_{0.9}InP_2S_6$ and 500 MHz at T = 330 K for $CuIn_{1+\delta}P_2S_6$ indicating a critical slowing down typical of the order–disorder ferroelectric phase transitions (Grigas, 1996). The frequency plot of the complex permittivity at different temperatures (Fig. 2) was fitted with the Cole–Cole formula:

$$\varepsilon^*(\omega) = \varepsilon_\infty + \frac{\Delta\varepsilon}{1+(i\omega\tau)^\alpha}, \tag{1}$$

where $\Delta\varepsilon$ represents the dielectric strength of the relaxation, τ is the mean Cole–Cole relaxation time, ε_∞ represents the contribution of all polar phonons and electronic polarization to the dielectric permittivity and a is the Cole–Cole relaxation time distribution parameter. *Eq.* (1) reduces to the Debye formula if $\alpha = 0$. The obtained parameters are presented in Fig. 3. At higher temperatures the α parameter is very small and indicates Debye type dielectric dispersion.

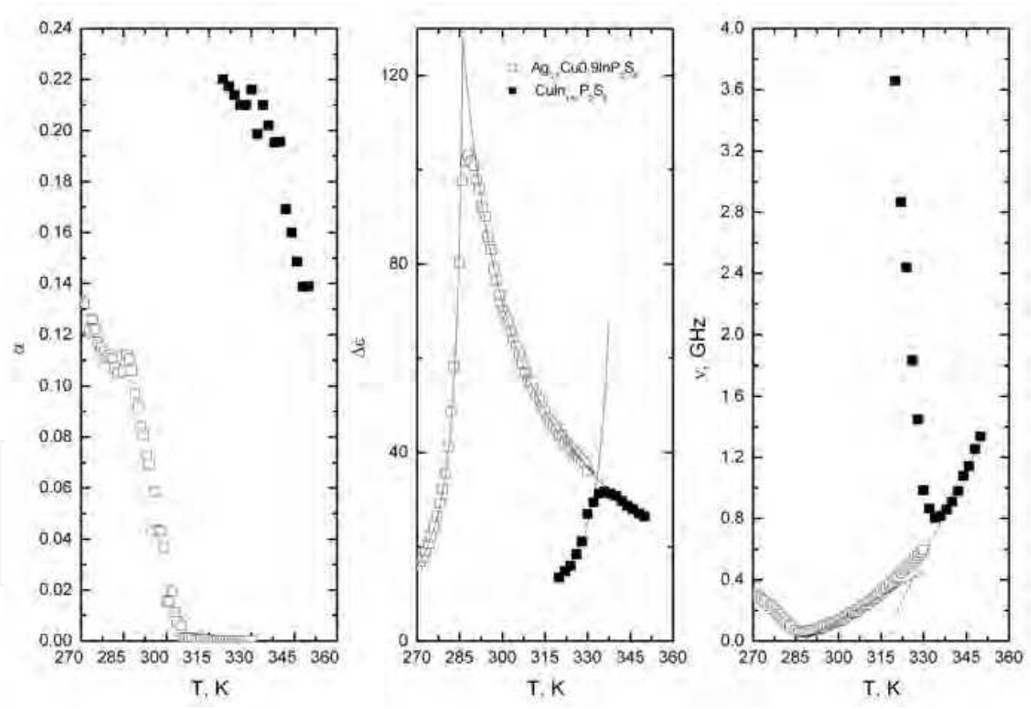

Fig. 3. Cole–Cole parameters of $Ag_{0.1}Cu_{0.9}InP_2S_6$ and $CuIn_{1+\delta}P_2S_6$ crystals.

On cooling the α parameter increases up to 0.133 for $Ag_{0.1}Cu_{0.9}InP_2S_6$ and 0.22 for $CuIn_{1+\delta}P_2S_6$ substantially below ferrielectric phase transition temperature T_c. The distribution of the relaxation times is much broader in the ferrielectric phase than in the paraelectric one. The temperature dependence of the dielectric strength $\Delta\varepsilon$ was fitted with the Curie–Weiss law:

$$\Delta\varepsilon = \frac{C_{p,f}}{\left|T - T_{Cp,Cf}\right|}, \tag{2}$$

where $C_{p,f}$ is the Curie–Weiss constant and $T_{Cp,Cf}$ is the Curie–Weiss temperature obtained from the fitting correspondingly in the paraelectric and ferrielectric phases. The ratios C_p/C_f = 7.8 (6.45 for $CuIn_{1+\delta}P_2S_6$), $C_p/T_{Cp} \approx 10$ (for both crystals) and mismatch T_{Cf}–T_{Cp} = 20 K (62 K for $CuIn_{1+\delta}P_2S_6$), show the first-order "order–disorder" ferroelectric phase transition. The temperature dependence of the mean Cole–Cole relaxation time τ in the paraelectric phase was fitted with the classical law (Grigas, 1996):

$$\tau = \tau_0 e^{U/kT} \frac{C_p}{T - T_{Cp}}, \tag{3}$$

where τ_0 is the relaxation time as $T \to \infty$ and the exponential factor describes deviations from phenomenological Landau theory close to the phase transition temperature, which appears due to critical fluctuations. The parameters obtained for $Ag_{0.1}Cu_{0.9}InP_2S_6$ are τ_0=8.1×10^{-16} s, U/k = 2980 K (0.26 eV).

2.2 Ferrielectric and dipolar glass phase coexistence in $CuInP_2S_6$ and $Ag_{0.1}Cu_{0.9}InP_2S_6$ crystals

At temperatures below 175 K dielectric dispersion effects can be observed at low frequencies for pure $CuInP_2S_6$ (Fig. 4). A similar dielectric dispersion also occurs in $Ag_{0.1}Cu_{0.9}InP_2S_6$ and in $CuIn_{1+\delta}P_2S_6$ at low temperatures. Such dielectric dispersion is typical of dipolar glasses (Figs. 4 and 5) (Macutkevic et al. 2008).

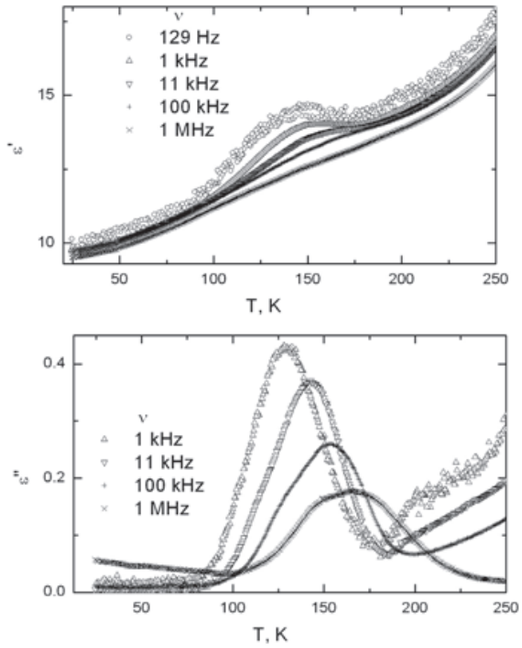

Fig. 4. Temperature dependence of the complex dielectric permittivity of $CuInP_2S_6$ crystals. Low temperature region.

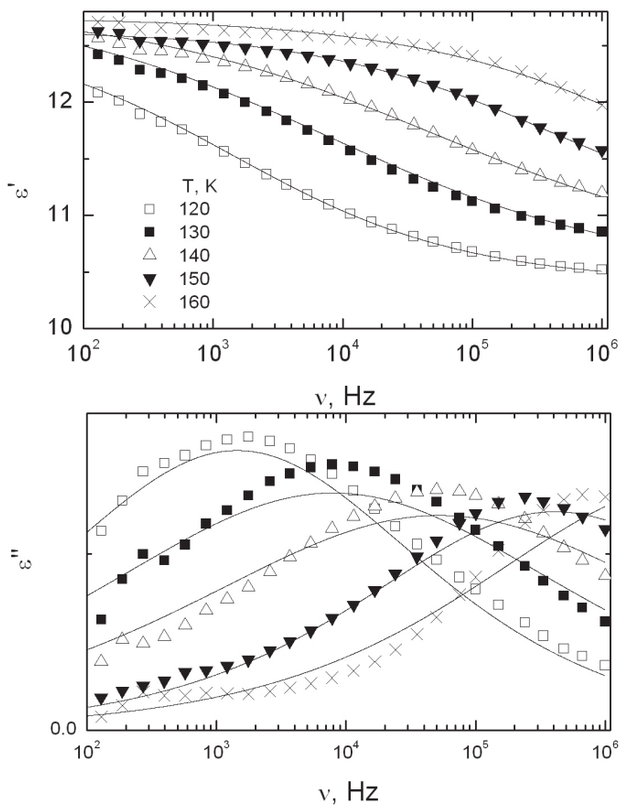

Fig. 5. Frequency dependence of the complex dielectric permittivity of $CuInP_2S_6$ crystals measured at different low temperatures. Solid lines are best fits to *Eq.* (1).

From dielectric spectra for $CuInP_2S_6$ and $Ag_{0.1}Cu_{0.9}InP_2S_6$ the Cole–Cole parameters were calculated. Very high and almost temperature independent value of the distribution of relaxation times α indicates a very wide distribution of relaxation times. The mean relaxation time increases on cooling according to the Vogel–Fulcher law:

$$\tau = \tau_0 \exp \frac{E_f}{k(T - T_0)} \tag{4}$$

where E_f is the activation energy and T_0 the freezing temperature. Obtained parameters are presented in (Dziaugys et al., 2010; Dziaugys et al., 2011). The freezing temperature is higher for $Ag_{0.1}Cu_{0.9}InP_2S_6$ as compared to $CuInP_2S_6$ and $CuIn_{1+\delta}P_2S_6$. What is the nature of dipole glass phase in pure $CuInP_2S_6$? First of all we must admit that the freezing occurs mainly in the copper sublattice, since the ferroelectric interaction exists only for copper ions in $CuInP_2S_6$. Secondly, in the dipole glass phase disorder should exist in the copper sublattice and competitive (ferroelectric and antiferroelectric) interactions occur between copper ions or (and) between copper ions and lattice. Competitive interactions can also occur between copper and indium ions. The static disorder in the copper sublattice was observed by X-ray investigations mainly at higher temperatures (Maisonneuve et al., 1997). This disorder is just random distribution of copper ions between more than the three positions (Cu^1, Cu^2, Cu^3). However, this is only a static picture of disorder in $CuInP_2S_6$. The dielectric spectroscopy

reveals that the dynamic disorder in $CuInP_2S_6$ does not vanish in the ferroelectric phase. The dynamic disorder is hopping of Cu ions between several possible static occupation positions. This hopping freezes at very low temperatures. The $CuInP_2S_6$ is a ferroelectric (ferrielectric) for which a dipole glass phase at low temperatures is observed even in the (nominally) pure crystal. Therefore $CuInP_2S_6$ with small amount of additions, independent from physical properties of the additions (ferroelectric, antiferroelectric or nonferroelectric) should exhibit the same phase diagram – the ferrielectric phase transition at higher temperatures and the freezing into a dipole glass phase at lower temperatures.

2.3 Phase transitions in antiferroelectric $CuCrP_2S_6$ and $CuIn_{0.1}Cr_{0.9}P_2S_6$ crystals

The antiferroelectric phase transition in $CuCrP_2S_6$ and $CuIn_{0.1}Cr_{0.9}P_2S_6$ is accompanied by a step-like dielectric anomaly (Fig. 6). The width of the step is approximately 5K for $CuCrP_2S_6$ and 20 K for $CuIn_{0.1}Cr_{0.9}P_2S_6$ Taking the temperature, corresponding to the peak point of the step as the temperature of phase transition, it was found that $T_c \approx 170$ K for $CuCrP_2S_6$ and 167 K for $CuIn_{0.1}Cr_{0.9}P_2S_6$.

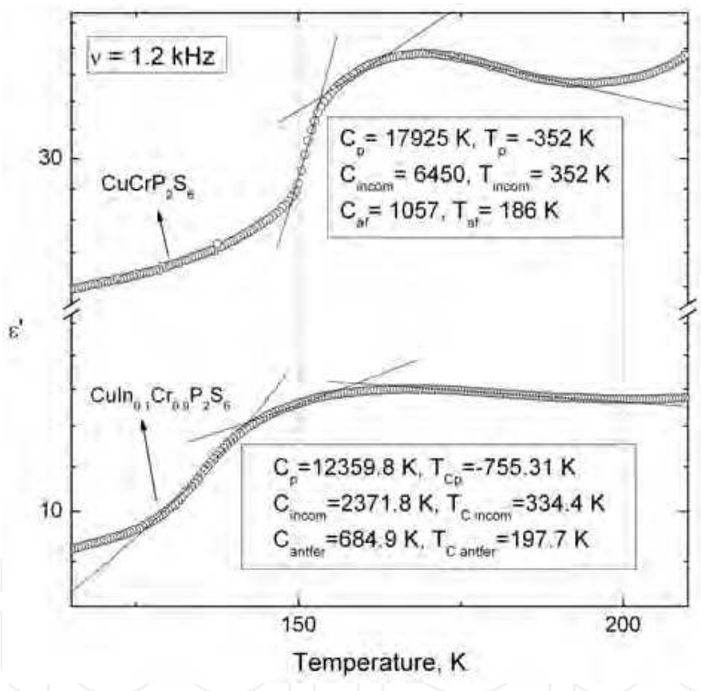

Fig. 6. Temperature dependence of the real part of the dielectric permittivity of a) $CuIn_{0.1}Cr_{0.9}P_2S_6$ and b) $CuInCrP_2S_6$. Solid lines are fitted according to the Curie – Weiss law.

While analyzing the sample from low temperatures, ε' rises slowly between 30 K and 125 K for $CuIn_{0.1}Cr_{0.9}P_2S_6$ and 150 K for $CuCrP_2S_6$, after which it increases abruptly and then smoothly, while at 167 K for $CuIn_{0.1}Cr_{0.9}P_2S_6$ and 170 K for $CuCrP_2S_6$ it starts decreasing. As we can see the ε' maximum is no so well pronounced as in $CuInP_2S_6$ (Banys et al., 2004), therefore such property is typical of antiferroelectrics (Kittel, 1951). The T width of this dielectric anomaly and the slope changes just below 167 K ($CuIn_{0.1}Cr_{0.9}P_2S_6$) and 170 K ($CuCrP_2S_6$) agree with the hypothesis of a slowly evolving short-range dipole order. Knowing that the copper dipole configuration is antipolar at T<150 K, we infer from the

relatively continuous decrease of ε' at 125 K ($CuIn_{0.1}Cr_{0.9}P_2S_6$) and 150 K ($CuInCrP_2S_6$) that the intermediate phase is quasi–antipolar (or incommensurate). It was found that $\varepsilon'(T)$ follows a Curie –Weiss law, *Eq.* (2). The ratio of $C_p/C_{af} >> 2$ indicates a first order phase transition to take place in both crystals.

2.4 Inhomogeneous ferrielectrics

The temperature dependence of the real and imaginary parts of the complex dielectric permittivity ε^* at various frequencies ν of $CuCr_{0.3}In_{0.7}P_2S_6$ crystals are presented in Fig. 7. We can see three different regions of dielectric dispersion. At temperatures T > 220 K and frequencies ν < 1 MHz the dielectric dispersion is mainly caused by the high conductivity, similarly as in pure $CuCrP_2S_6$ and $CuInP_2S_6$ crystals. The dielectric dispersion caused by the relaxation soft mode is observed in the vicinity of the ferroelectric phase transition temperature $T_c \approx 256$ K for $CuCr_{0.3}In_{0.7}P_2S_6$ and $T_c \approx 247$ K for $CuCr_{0.2}In_{0.8}P_2S_6$ and at higher frequencies (ν > 1 MHz). The dispersion at low temperatures (T < 170 K) is characteristic of the freezing into the dipole glass state. It is likely that substitutions in the chromium sublattice give rise to a more complex potential relief in which the copper ions move. As a consequence a part of the copper ions does not participate in the cooperative dynamics involved in the ferroelectric ordering. The dependence of the dielectric permittivity on frequency has been fitted with the Cole-Cole formula. The parameter $\Delta\varepsilon$ in the vicinity of the ferroelectric phase transition temperature follows the Curie-Weiss law, *Eq.* 2. To find out its order we have calculated the Curie-Weiss constants in the paraelectric and ferroelectric phases, respectively: $C_p \approx 4940$ K and $C_f \approx 2580$ K. From the ratio of these constants (1.92) it is clear that crystal with x = 0.7 undergoes a second-order phase transition. The ratio $C_{p,f}/T_C$ is in the order 10, therefore the observed phase transition is mainly of the "order-disorder" type (Grigas, 1996). The Cole-Cole mean relaxation time τ increases with decreasing temperature, according to the Vogel-Fulcher law. No anomaly of the relaxation time is

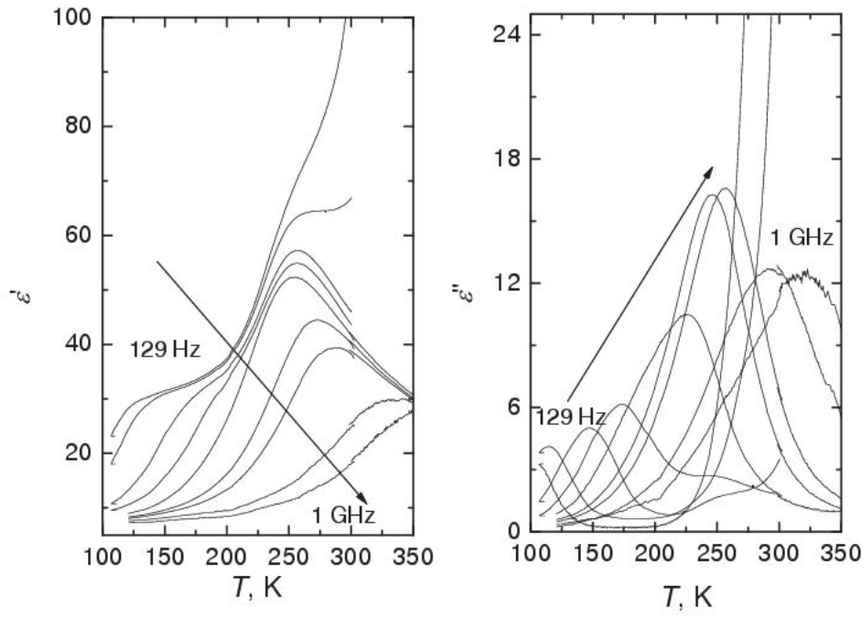

Fig. 7. Temperature dependence of the complex dielectric permittivity of $CuCr_{0.3}$ $In_{0.7}CrP_2S_6$

observed in the vicinity of the ferroelectric phase transition. In order to get information that is more precise about the relaxation-time distribution function, a special approach has been developed. A detailed description can be found in (Banys et al., 2002). We assume that the complex dielectric spectrum $\varepsilon^*(\nu)$ can be represented as a superposition of independent individual Debye-type relaxation processes (Schafer et al., 1996; Kim et al., 2000; Pelster et al., 1998)

$$\varepsilon^*(\nu) = \varepsilon_\infty + \Delta\varepsilon \int_{-\infty}^{\infty} \frac{f(\tau) d\lg\tau}{1 + i\omega\tau}. \tag{4}$$

The distributions of relaxation times of the investigated ferrielectric $CuCr_{0.3}In_{0.7}P_2S_6$ are presented in Fig. 8. One can recognize that the relaxation-time distribution function significantly broadens at low temperatures, as it is typical for dipole glasses. Let us consider the copper ions moving in asymmetric double well potentials. The movement consists of fast oscillations in one of the minima with occasional thermally activated jumps between the minima. The jump probability is governed by the Boltzmann probability of overcoming the potential barrier between the minima. The relaxation time in such a system is given by:

$$\tau = \tau_0 \frac{\exp[E_b / k_B(T - T_0)]}{2\cosh(A / 2k_B T)}. \tag{5}$$

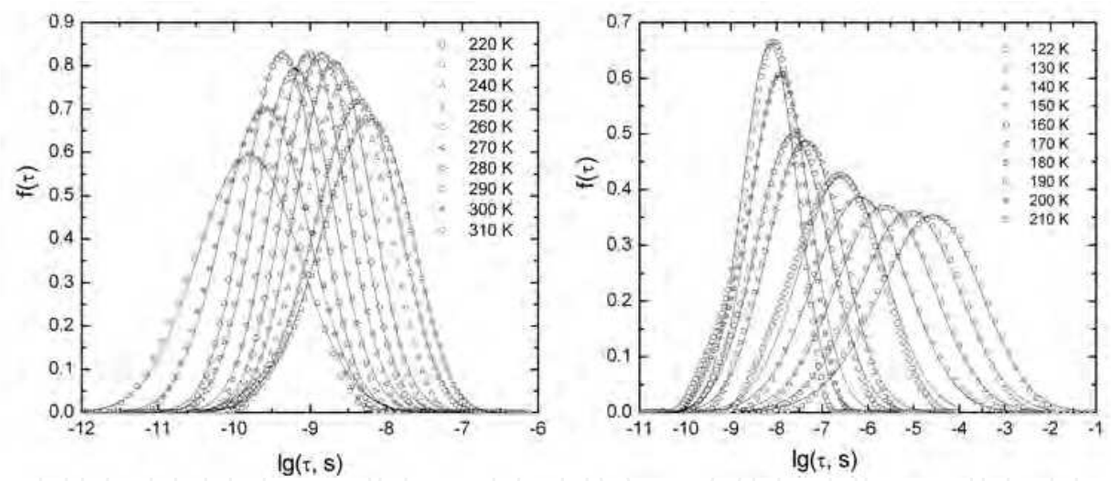

Fig. 8. Distribution of relaxation times of mixed ferroelectric $Cu(In_{0.7}Cr_{0.3})P_2S_6$ obtained from dielectric spectra (points). The solid lines are best fits according to *Eq.* (4).

The parameter A accounts for the asymmetry of the local potential produced by the mean-field influence of all the other dipoles. Thus, the local polarization of copper ions is

$$p = \tanh(A / 2k_B T) \tag{6}$$

and the distribution function $\varpi(p)$ of the local polarizations:

$$\varpi(p) = \frac{2k_B T}{\sqrt{2\pi}\sigma_A(1 - p^2)} \exp\left[-\frac{(a\tanh[p] - a\tanh[\bar{p}])^2}{2\sigma_A(2k_B T)^2} \right]. \tag{7}$$

We further consider that the asymmetry A and the potential barrier E_b of the local potential are randomly distributed around their mean values A_0 and E_{b0} according to a Gaussian law resulting in the distribution functions:

$$f(E_b) = \frac{1}{\sqrt{2\pi}\sigma_{Eb}} \exp\left(-\frac{(E_b - E_{b0})^2}{2\sigma_{Eb}^2}\right) \tag{8}$$

with

$$f(A) = \frac{1}{\sqrt{2\pi}\sigma_A} \exp\left(-\frac{(A - A_0)^2}{2\sigma_A^2}\right), \tag{9}$$

where σ_{Eb} and σ_A are the standard deviations of E_b and A, respectively, from their mean values. Fits with the experimentally obtained relaxation-time distributions were performed and the results are presented in Fig. 8 as solid lines. Knowing the average asymmetry A and the standard deviation of asymmetry σ_A we have calculated the distributions of local polarization $w(p)$ (Fig. 9).

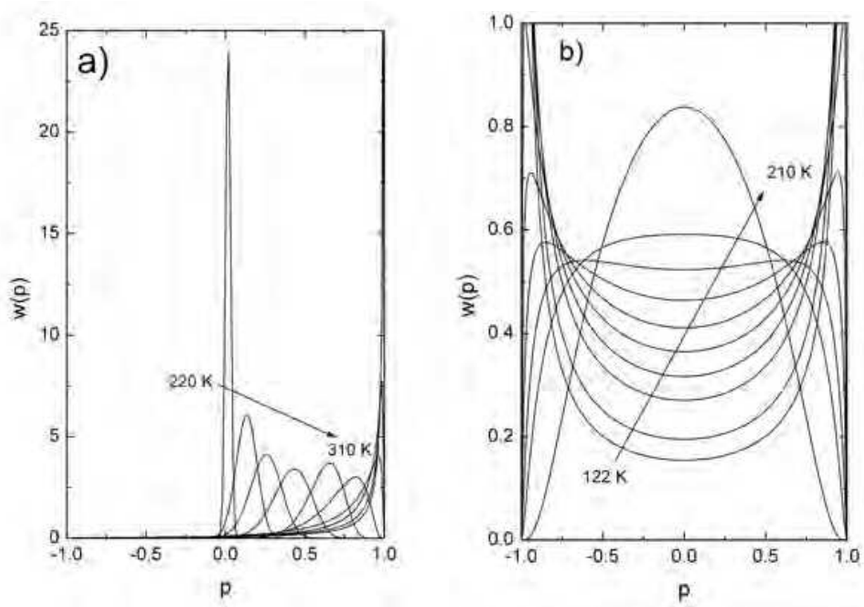

Fig. 9. Distribution of local polarizations $w(p)$ of a $CuCr_{0.3}In_{0.7}P_2S_6$ crystal: at several temperatures.

A broad distribution of local polarization is observed in both investigated ferrielectrics are typical for inhomogeneous ferroelectrics. It indicates that not all copper ions are ordered in the ferrielectric phase. This fact was confirmed also by X ray investigations of pure $CuInP_2S_6$. By further cooling non-ordered copper ions form a glassy phase and finally become frozen. Knowing the distribution function $w(p)$, both the average (macroscopic) polarization

$$\overline{p} = \int_{-1}^{1} p w(p) dp \tag{10}$$

and the Edwards-Anderson glass order parameter

$$q_{EA} = \int_{-1}^{1} p^2 w(p) dp \tag{11}$$

can be calculated (Fig. 10). The temperature behavior of the average polarization is typical for the second-order ferroelectric phase transition.

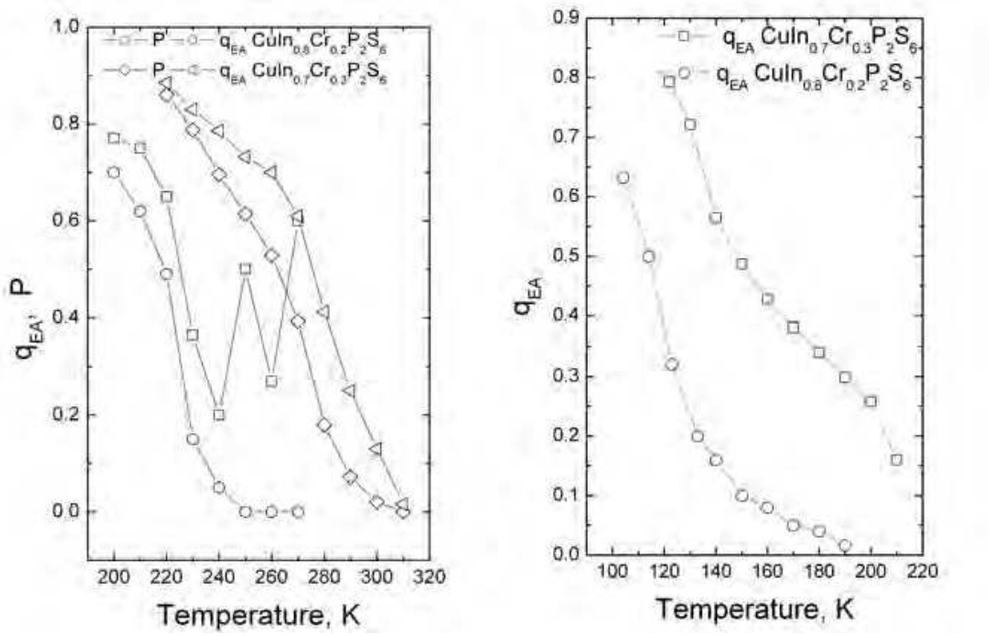

Fig. 10. Temperature dependence of the spontaneous polarization P and the Edwards-Anderson parameter q_{EA} of mixed $CuCr_{0.2}In_{0.8}P_2S_6$ and $CuCr_{0.3}In_{0.7}P_2S_6$ crystals.

2.5 Dipole glass state in mixed $CuCr_{1-x}In_xP_2S_6$ crystal

The temperature dependence of the dielectric properties in the $CuCr_{1-x}In_xP_2S_6$ mixed crystals with x = 0.5 is presented in Fig. 11. The shoulder-like $\varepsilon'(T)$ anomaly shifts toward higher temperatures with increasing frequency. The dielectric relaxation is also expressed in the dielectric losses. The dielectric dispersion at low temperatures (T < 170 K) is typical of dipole glasses. At higher temperatures the dielectric dispersion is clearly symmetric and observed only at higher frequencies. On cooling it strongly passes to lower frequencies and becomes more asymmetric. The dielectric dispersion is described with the Cole-Cole formula. The Cole-Cole mean relaxation time τ increases with decreasing temperature, according to the Vogel-Fulcher law, the parameters of which are noticed in Table 2.

	$CuIn_{0.5}Cr_{0.5}P_2S_6$	$CuIn_{0.4}Cr_{0.6}P_2S_6$
T_0, K	23	20
E/k, K (eV)	1554 (0.134)	1575 (0.136)
τ_0, s	$7.67 \cdot 10^{-13}$	$4.7 \cdot 10^{-13}$

Table 2. Parameters of the Vogel–Fulcher law.

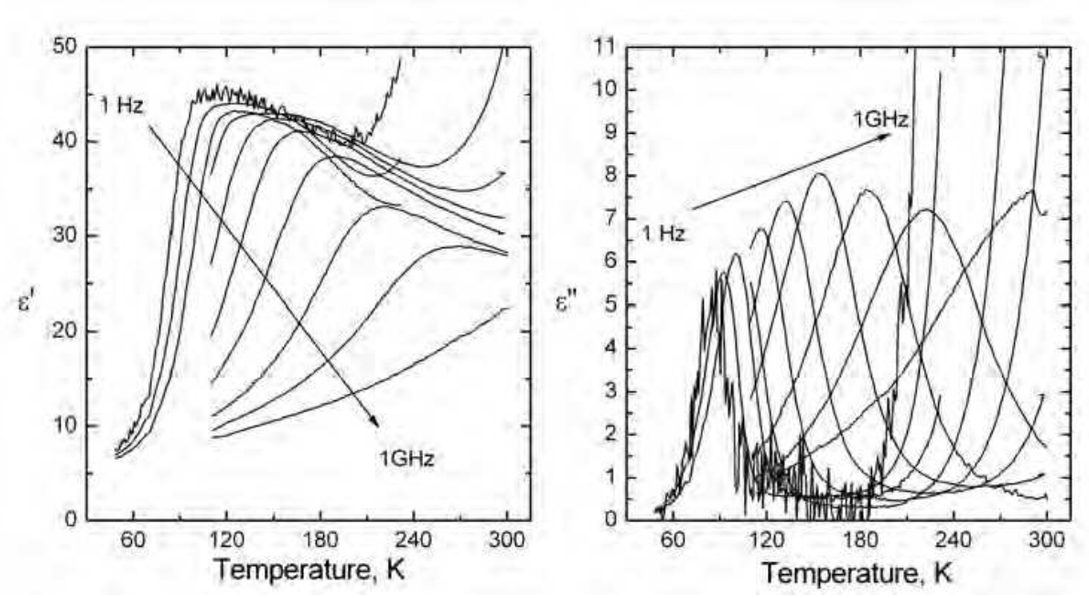

Fig. 11. Temperature dependence of the complex dielectric permittivity of $CuIn_{0.5}Cr_{0.5}CrP_2S_6$

Broad and very asymmetric distributions of relaxation times are observed in both investigated dipolar glasses (Fig. 12). To get more insight into the nature of such distributions, they are fitted by the double well potential model described above.

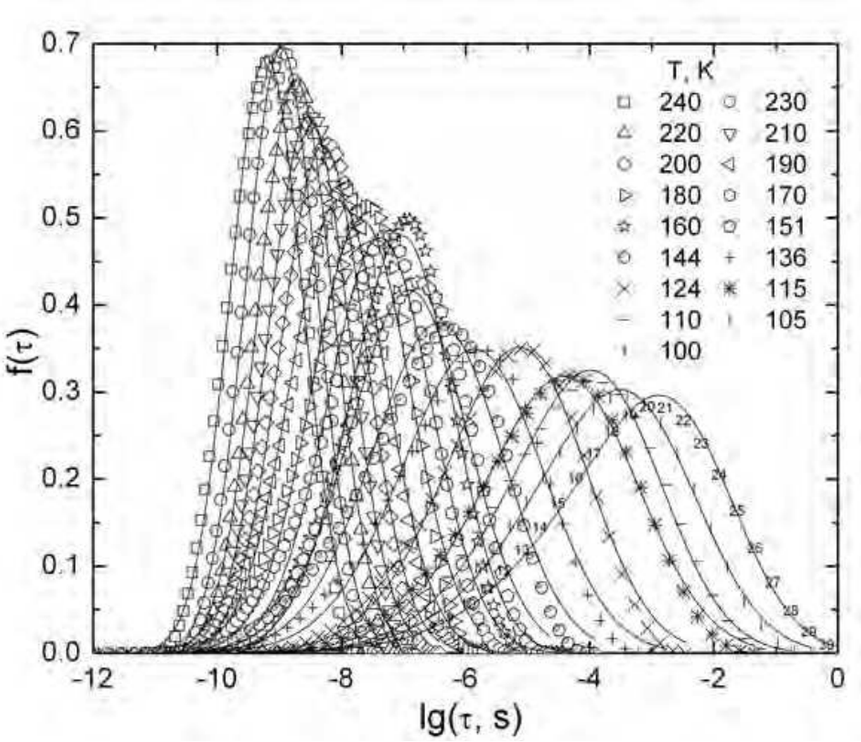

Fig. 12. Distribution of relaxation times of ferroelectric $CuCr_{0.5}In_{0.5}P_2S_6$

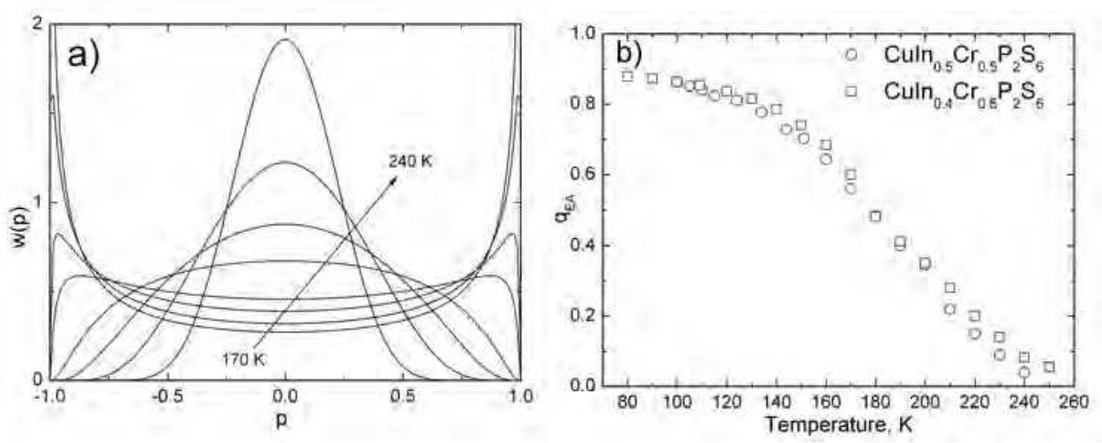

Fig. 13. a) Distribution of local polarizations $w(p)$ of $CuCr_{0.5}In_{0.5}P_2S_6$ at several temperatures. b) Temperature dependence of the Edwards-Anderson parameter of mixed $CuCr_{0.5}In_{0.5}P_2S_6$ and $CuCr_{0.6}In_{0.4}P_2S_6$ crystals.

From the double well potential parameters the local polarization distribution has been calculated (Fig. 13). The temperature behavior of the local polarization distribution is very similar to that of other dipole glasses like RADP or BP/BPI (Banys et al., 1994). The order parameter is an almost linear function of the temperature and does not indicate any anomaly.

2.6 Phase diagram of the mixed $CuIn_xCr_{1-x}P_2S_6$ crystals

The phase diagram of $CuCr_{1-x}In_xP_2S_6$ mixed crystals obtained from our dielectric results is shown in Fig. 14. Ferroelectric ordering coexisting with a dipole glass phase in $CuCr_{1-x}In_xP_2S_6$ is present for $0.7 \leq x$. On the other side of the phase diagram for $x \leq 0.9$ the antiferroelectric phase transition occurs. At decreasing concentration x the antiferroelectric phase transition temperature increases. In the intermediate concentration range for $0.4 \leq x \leq 0.6$, dipolar glass phases are observed.

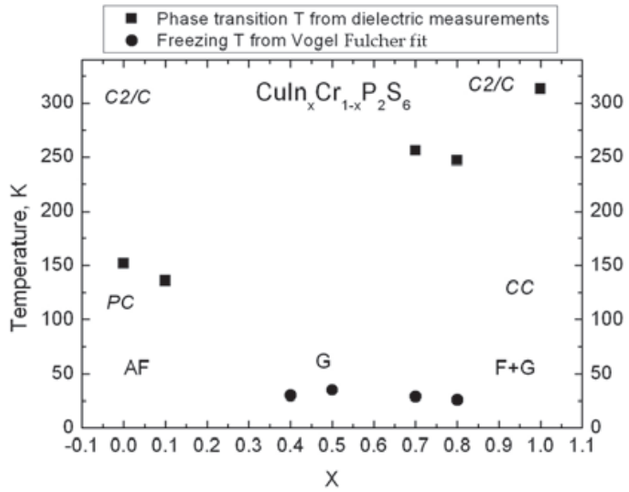

Fig. 14. Phase diagram of $CuCr_{1-x}In_xP_2S_6$ crystals. AF – antiferroelectric phase; G – glass phase; F+G – ferroelectric + glass phase.

3. Magnetic properties of $CuCr_{1-x}In_xP_2S_6$ single crystals

3.1 Experimental procedure

Single crystals of $CuCr_{1-x}In_xP_2S_6$, with x = 0, 0.1, 0.2, 0.4, 0.5, and 0.8 were grown by the Bridgman method and investigated as thin as-cleft rectangular platelets with typical dimensions 4×4×0.1 mm^3. The long edges define the *ab*-plane and the short one the *c*-axis of the monoclinic crystals (Colombet et al., 1982). While the magnetic easy axis of the x = 0 compound lies in the *ab*-plane (Colombet et al., 1982), the spontaneous electric polarization of the x = 1 compound lies perpendicular to it (Maisonneuve et al., 1997).

Magnetic measurements were performed using a SQUID magnetometer (Quantum Design MPMS-5S) at temperatures from 5 to 300 K and magnetic fields up to 5 T. For magneto-electric measurements we used a modified SQUID *ac* susceptometer (Borisov et al., 2007), which measures the first harmonic of the *ac* magnetic moment induced by an external *ac* electric field. To address higher order ME effects, additional *dc* electric and/or magnetic bias fields are applied (Shvartsman et al., 2008).

3.2 Temperature dependence of the magnetization

The temperature (T) dependence of the magnetization (M) measured on $CuCr_{1-x}In_xP_2S_6$ samples with x = 0, 0.1, 0.2, 0.4, 0.5 and 0.8 in a magnetic field of $\mu_0 H$ = 0.1 T applied perpendicularly to the *ab*-plane are shown in Fig. 15a within 5 ≤ T ≤ 150 K. Cusp-like AF anomalies are observed for x = 0, 0.1, and 0.2, at T_N ≈ 32, 29, and 23 K, respectively, as displayed in Fig. 15. While Curie-Weiss-type hyperbolic behavior, $M \propto (T - \Theta)^{-1}$, dominates above the cusp temperatures (Colombet et al., 1982), near constant values of M are found as $T \rightarrow 0$. They remind of the susceptibility of a uniaxial antiferromagnet perpendicularly to its easy axis, $\chi_\perp \approx const.$, thus confirming its assertion for $CuCrP_2S_6$ (Colombet et al., 1982).

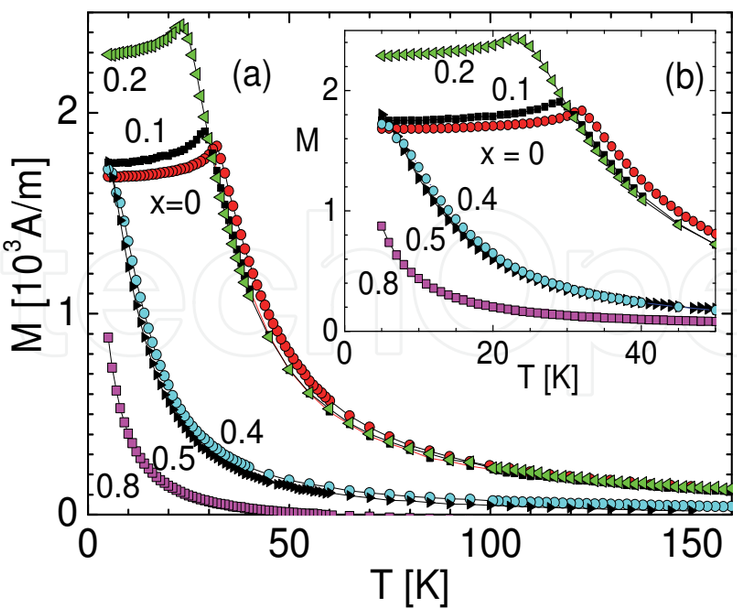

Fig. 15. Magnetization M *vs.* temperature T obtained for $CuCr_{1-x}In_xP_2S_6$ with x = 0, 0.1, 0.2, 0.4, 0.5, and 0.8 in $\mu_0 H$ = 0.1 T applied parallel to the *c* axis before (a) and after correction for the diamagnetic underground (b; see text).

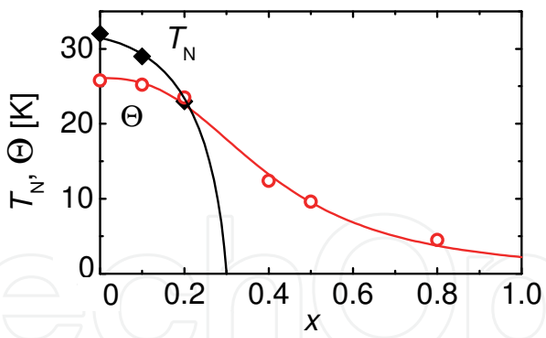

Fig. 16. Néel and Curie temperatures, T_N and Θ, *vs.* In^{3+} concentration x, derived from Fig. 15 (M) and Fig. 17 ($1/M$), and fitted by parabolic and logistic decay curves (solid lines), respectively.

At higher In^{3+} contents, $x \geq 0.4$, no AF cusps appear any more and the monotonic increase of M on cooling extends to the lowest temperatures, $T \approx 5$ K. Obviously the Cr^{3+} concentration falls short of the percolation threshold of the exchange interaction paths between the Cr^{3+} spins, which probably occurs at $x \approx 0.3$.

A peculiarity is observed at the highest In^{3+} concentration, $x = 0.8$ (Fig. 15a). The magnetization assumes negative values as $T > 60$ K. This is probably a consequence of the diamagnetism of the In^{3+} sublattice, the constant negative magnetization of which becomes dominant at elevated temperatures. For an adequate evaluation of the Cr^{3+} driven magnetism we correct the total magnetic moments for the diamagnetic background via the function

$$M = \frac{C}{T - \Theta} + D \,. \tag{12}$$

This model function accounts for pure Curie-Weiss behavior with the constant C at sufficiently high temperature and for the corresponding diamagnetic background D at all compositions. Table 3 presents the best-fit parameters obtained in individual temperature ranges yielding highest coefficients of determination, R^2. As can be seen, all of them exceed 0.999, hence, excellently confirming the suitability of *Eq.* (12). The monotonically decreasing magnitudes of the negative background values $D \approx -53$, -31, and -5 A/m for $x = 0.8$, 0.5, and 0.4, respectively, reflect the increasing ratio of paramagnetic Cr^{3+} *vs.* diamagnetic In^{3+} ions. We notice that weak negative background contributions, $D \approx -17$ A/m, persist also for the lower concentrations, $x = 0.2$, 0.1 and 0. Presumably the diamagnetism is here dominated by the other diamagnetic unit cell components, *viz.* S_6 and P_2.

x	Θ [K]	C [10^3A/(m·K)]	D [A/m]	best-fitting range	R^2
0	25.8±0.2	20.72±0.22	-28.7±2.2	T ≥ 50 K	0.9999
0.1	25.2±0.2	18.16±0.16	-16.4±0.9	T ≥ 45 K	0.9994
0.2	23.5±0.2	19.53±0.13	-16.6±1.0	T ≥ 45 K	0.9997
0.4	12.4±0.2	6.56±0.06	-4.5±0.4	T ≥ 34 K	0.9998
0.5	9.6±0.3	6.99±0.10	-31.4±0.4	T ≥ 29 K	0.9994
0.8	4.5±0.1	3.19±0.02	-54.6±0.3	T ≥ 21 K	0.9998

Table 3. Best-fit parameters of the data in Fig. 15 to *Eq.* (12).

Remarkably, the positive, *i.e.* FM Curie-Weiss temperatures, $26 > \Theta > 23$ K, for $0 \le x \le 0.2$ decrease only by 8%, while the decrease of T_N is about 28% (Fig. 16). This indicates that the two-dimensional (2D) FM interaction within the *ab* layers remains intact, while the interplanar AF coupling becomes strongly disordered and, hence, weakened such that T_N decreases markedly. It is noticed that our careful data treatment revises the previously reported near equality, $\Theta \approx T_N \approx 32$ K for $x = 0$ (Colombet et al., 1982). Indeed, the secondary interplanar exchange constant, J_{inter}/k_B = - 1K, whose magnitude is not small compared to the FM one, J_{intra}/k_B = 2.6 K (Colombet et al., 1982), is expected to drive the crossover from 2D FM to 3D AF 'critical' behavior far above the potential FM ordering temperature, Θ.

As can be seen from Table 3 and from the intercepts with the T axis of the corrected $1/M$ *vs.* T plots in Fig. 17, the Curie-Weiss temperatures attain positive values, $\Theta > 0$, also for high concentrations, $0.4 \le x \le 0.8$. This indicates that the prevailing exchange interaction remains FM as in the concentrated antiferromagnet, $x = 0$ (Colombet et al., 1982). However, severe departures from the straight line behavior at low temperatures, $T < 30$ K, indicate that competing AF interactions favour disordered magnetism rather than pure paramagnetic behavior. Nevertheless, as will be shown in Fig. 19 for the $x = 0.5$ compound, glassy freezing with non-ergodic behavior (Mydosh, 1995) is not perceptible, since the magnetization data are virtually indistinguishable in zero-field cooling/field heating (ZFC-FH) and subsequent field cooling (FC) runs, respectively.

The concentration dependences of the characteristic temperatures, T_N and Θ, in Fig. 16 confirm that the system $CuCr_{1-x}In_xP_2S_6$ ceases to become globally AF at low T for dilutions $x > 0.3$, but continues to show preponderant FM interactions even as $x \to 1$. The tentative percolation limit for the occurrence of AF long-range order as extrapolated in Fig. 16 is reached at $x_p \approx 0.3$. This is much lower than the corresponding value of $Fe_{1-x}Mg_xCl_2$, $x_p \approx 0.5$ (Bertrand et al., 1984). Also at difference from this classic dilute antiferromagnet we find a stronger than linear decrease of T_N with x. This is probably a consequence of the dilute magnetic occupancy of the cation sites in the $CuCrP_2S_6$ lattice (Colombet et al., 1982), which breaks intraplanar percolation at lower x than in the densely packed Fe^{2+} sublattice of $FeCl_2$ (Bertrand et al., 1984).

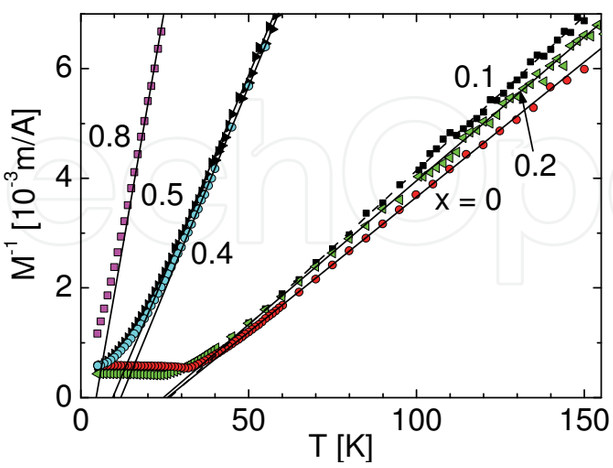

Fig. 17. Inverse magnetization M^{-1} corrected for diamagnetic background, *Eq.* (12), *vs.* T taken from Fig. 15 (inset). The straight lines are best-fitted to corrected Curie-Weiss behavior, *Eq.* (12), within individual temperature ranges (Table 3). Their abscissa intercepts denote Curie temperatures, Θ (Table 3).

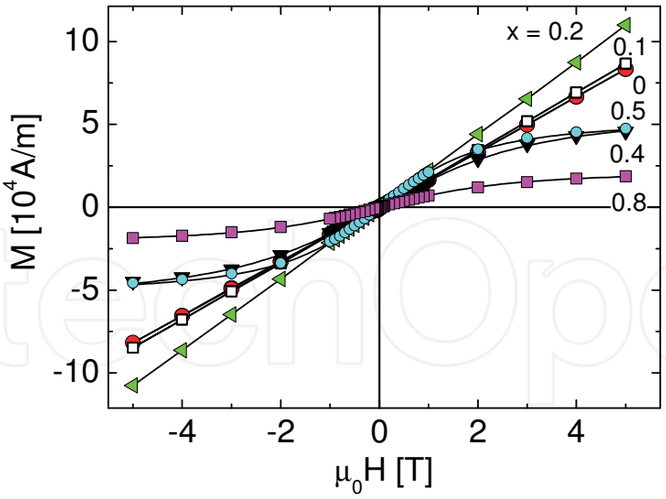

Fig. 18. Out-of-plane magnetization of $CuCr_{1-x}In_xP_2S$ with $0 \le x \le 0.8$ recorded at $T = 5$ K in magnetic fields $|\mu_0 H| \le 5$ T. The straight solid lines are compatible with $x = 0$, 0.1, and 0.2, while Langevin-type solid lines, *Eq.* (14) and Table 4, deliver best-fits for $x = 0.4$, 0.5, and 0.8.

A sigmoid logistic curve describes the decay of the Curie temperature in Fig. 16,

$$\Theta = \frac{\Theta_0}{1 + (x/x_0)^p}, \tag{13}$$

with best-fit parameters $\Theta_0 = 26.1$, $x_0 = 0.405$ and $p = 2.63$. It characterizes the decay of the magnetic long-range order into 2D FM islands, which rapidly accelerates for $x > x_0 \approx x_p \approx 0.3$, but sustains the basically FM coupling up to $x \to 1$.

3.3 Field dependence of the magnetization

The magnetic field dependence of the magnetization of the $CuCr_{1-x}In_xP_2S$ compounds yields additional insight into their magnetic order. Fig. 18 shows FC out-of-plane magnetization curves of samples with $0 \le x \le 0.8$ taken at $T = 5$ K in fields $-5 \text{ T} \le \mu_0 H \le 5$ T. Corrections for diamagnetic contributions as discussed above have been employed. For low dilutions, $0 \le x \le 0.2$, non-hysteretic straight lines are observed as expected for the AF regime (see Fig. 15) below the critical field towards paramagnetic saturation. Powder and single crystal data on the $x = 0$ compound are corroborated except for any clear signature of a spin-flop anomaly, which was reported to provide a slight change of slope at $\mu_0 H_{SF} \approx 0.18$ T (Colombet et al., 1982). This would, indeed, be typical of the easy *c*-axis magnetization of near-Heisenberg antiferromagnets like $CuCrP_2S$, where the magnetization components are expected to rotate jump-like into the *ab*-plane at $\mu_0 H_{SF}$. This phenomenon was thoroughly investigated on the related lamellar MPS_3-type antiferromagnet, $MnPS_3$ albeit at fairly high fields, $\mu_0 H_{SF} \approx 4.8$ T (Goossens et al., 2000), which is lowered to 0.07 T for diamagnetically diluted $Mn_{0.55}Zn_{0.45}PS_3$ (Mulders et al., 2002).

In the highly dilute regime, $0.4 \le x \le 0.8$, the magnetization curves show saturation tendencies, which are most pronounced for $x = 0.5$, where spin-glass freezing might be expected as reported *e.g.* for $Fe_{1-x}Mg_xCl_2$ (Bertrand et al., 1984). However, no indication of hysteresis is visible in the data. They turn out to excellently fit Langevin-type functions,

$$M(H) = M_0 \left[\coth(y) - 1/y\right], \tag{14}$$

where $y = (m\mu_0 H)/(k_B T)$ with the 'paramagnetic' moment m and the Boltzmann constant k_B. Fig. 18 shows the functions as solid lines, while Table 4 summarizes the best-fit results.

x	M_0	m	$N = M_0/m$
0.4	65.7 kA/m	5.6×10^{-23} Am² = 6.1μ_B	1.2 nm^{-3}
0.5	59.6 kA/m	8.5×10^{-23} Am² = 9.2μ_B	0.7 nm^{-3}
0.8	24.7 kA/m	6.86×10^{-23} Am² = 7.4μ_B	0.4 nm^{-3}

Table 4. Best-fit parameters of data in Fig. 18 to *Eq.* (14).

While the saturation magnetization M_0 and the moment density N scale reasonably well with the Cr^{3+} concentration, 1-x, the 'paramagnetic' moments exceed the atomic one, $m(Cr^{3+})$ = 4.08 μ_B (Colombet et al., 1982) by factors up to 2.5. This is a consequence of the FM interactions between nearest-neighbor moments. They become apparent at low T and are related to the observed deviations from the Curie-Weiss behavior (Fig. 17). However, these small '*superparamagnetic*' clusters are obviously not subject to blocking down to the lowest temperatures as evidenced from the ergodicity of the susceptibility curves shown in Fig. 15.

3.4 Anisotropy of magnetization and susceptibility

The cluster structure delivers the key to another surprising discovery, namely a strong anisotropy of the magnetization shown for the x = 0.5 compound in Fig. 19. Both the isothermal field dependences $M(H)$ at T = 5 K (Fig. 19a) and the temperature dependences $M(T)$ shown for $\mu_0 H$ = 0.1 T (Fig. 19b) split up under different sample orientations. Noticeable enhancements by up to 40% are found when rotating the field from parallel to perpendicular to the c-axis. At T = 5 K we observe $M_\perp \approx 70$ and 2.5 kA/m *vs.* $M_\parallel \approx 50$ and 1.8 kA/m at $\mu_0 H$ = 5 and 0.1 T, respectively (Fig. 19a and b).

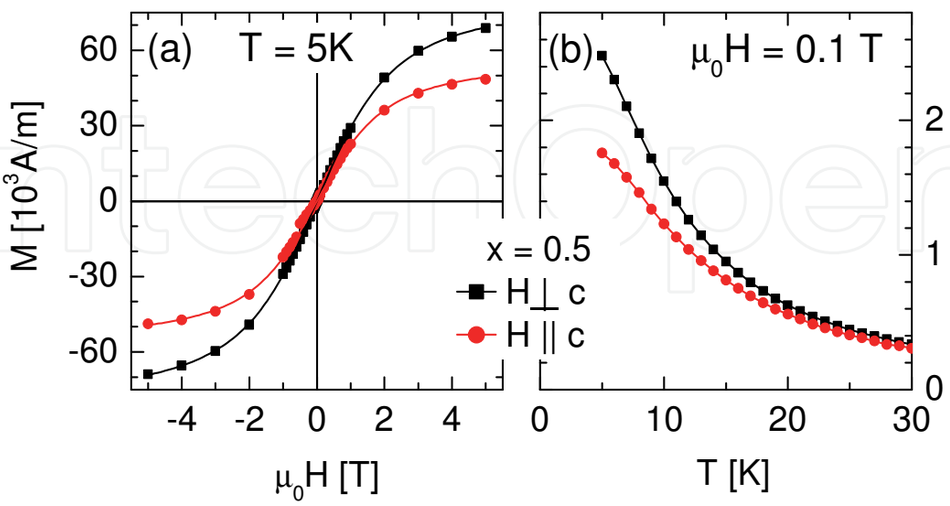

Fig. 19. Magnetization M of $CuCr_{0.5}In_{0.5}P_2S_6$ measured parallel (red circles) and perpendicularly (black squares) to the c axis (a) *vs.* $\mu_0 H$ at T = 5 K (best-fitted by Langevin-type solid lines) and (b) *vs.* T at $\mu_0 H$ = 0.1T (interpolated by solid lines).

At first sight this effect might just be due to different internal fields, $H^{int} = H - NM$, where N is the geometrical demagnetization coefficient. Indeed, from our thin sample geometry, 3×4×0.03 mm^3, with $N_\parallel \approx 1$ and $N_\perp << 1$ one anticipates $H_\parallel{}^{int} < H_\perp{}^{int}$, hence, $M_\parallel < M_\perp$. However, the demagnetizing fields, $N_\perp M_\perp \approx 0$ and $N_\parallel M_\parallel \approx 50$ and 1.8 kA/m, are no larger than 2% of the applied fields, H = 4 MA/m and 80 kA/m, respectively. These corrections are, hence, more than one order of magnitude too small as to explain the observed splittings. Since the anisotropy occurs in a paramagnetic phase, we can also not argue with AF anisotropy, which predicts $\chi_\perp > \chi_\parallel$ at low T (Blundell, 2001). We should rather consider the intrinsic magnetic anisotropy of the above mentioned 'superparamagnetic' clusters in the layered $CuCrP_2S_6$ structure. Their planar structure stems from large FM in-plane correlation lengths, while the AF out-of-plane correlations are virtually absent. This enables the magnetic dipolar interaction to support in-plane FM and out-of-plane AF alignment in $H_\perp$, while this spontaneous ordering is weakened in $H_\parallel$. However, the dipolar anisotropy cannot explain the considerable difference in the magnetizations at saturation, $M_0\parallel$=58.5 kA/m and $M_0{}^\perp$ = 84.2 kA/m, as fitted to the curves in Fig. 19a. This strongly hints at a mechanism involving the total moment of the Cr^{3+} ions, which are subject to orbital momentum transfer to the spin-only $^4A_2(d^3)$ ground state. Indeed, in the axial crystal field zero-field splitting of the $^4A_2(d^3)$ ground state of Cr^{3+} is expected, which admixes the $^4T_{2g}$ excited state via spin-orbit interaction (Carlin, 1985). The magnetic moment then varies under different field directions as the gyrotropic tensor components, $g_\perp$ and $g\parallel$, while the susceptibilities follow $g_\perp{}^2$ and $g\parallel{}^2$, respectively. However, since $g_\perp$ = 1.991 and $g\parallel$ = 1.988 (Colombet et al., 1982) the single-ion anisotropies of both M and χ are again mere 2% effects, unable to explain the experimentally found anisotropies.

Since single ion properties are not able to solve this puzzle, the way out of must be hidden in the collective nature of the 'superparamagnetic' Cr^{3+} clusters. In view of their intrinsic exchange coupling we propose them to form 'molecular magnets' with a high spin ground states accompanied by large magnetic anisotropy (Bogani & Wernsdörfer, 2008) such as observed on the AF molecular ring molecule Cr_8 (Gatteschi et al., 2006). The moderately enhanced magnetic moments obtained from Langevin-type fits (Table 4) very likely refer to mesoscopic 'superantiferromagnetic' clusters (Néel, 1961) rather than to small 'superparamagnetic' ones. More experiments, in particular on time-dependent relaxation of the magnetization involving quantum tunneling at low T, are needed to verify this hypothesis.

It will be interesting to study the concentration dependence of this anisotropy in more detail, in particular at the percolation threshold to the AF phase. Very probably the observation of the converse behavior in the AF phase, $\chi_\perp < \chi_\parallel$ (Colombet et al., 1982), is crucially related to the onset of AF correlations. In this situation the anisotropy will be modified by the spin-flop reaction of the spins to $H_\parallel$, where $\chi_\parallel$ jumps up to the large $\chi_\perp$ and both spin components rotate synchronously into the field direction.

3.5 Magnetoelectric coupling

Magnetic and electric field-induced components of the magnetization, $\boldsymbol{M} = \boldsymbol{m}/V$,

$$\mu_0 M_i = -\partial F / \partial H_i = \mu_0 \mu_{ij} H_j + \alpha_{ij} E_j + \beta_{ijk} E_j H_k + \frac{\gamma_{ijk}}{2} E_j E_k + \delta_{ijkl} H_j E_k E_l \,, \tag{15}$$

related to the respective free energy under Einstein summation (Shvartsman et al., 2008)

$$F(\mathbf{E},\mathbf{H}) = F_0 - \frac{1}{2}\varepsilon_0\varepsilon_{ij}E_iE_j - \frac{1}{2}\mu_0\mu_{ij}H_iH_j - \alpha_{ij}H_iE_j - \frac{\beta_{ijk}}{2}H_iE_jH_k - \frac{\gamma_{ijk}}{2}H_iE_jE_k - \frac{\delta_{ijkl}}{2}H_iH_jE_kE_l \quad (16)$$

were measured using an adapted SQUID susceptometry (Borisov et al., 2007). Applying external electric and magnetic *ac* and *dc* fields along the monoclinic [001] direction, $E = E_{ac}\cos\omega t + E_{dc}$ and H_{dc}, the real part of the first harmonic *ac* magnetic moment at a frequency $f = \omega/2\pi = 1$ Hz,

$$m'_{ME} = (a_{33}E_{ac} + \beta_{333}E_{ac}H_{dc} + \gamma_{333}E_{ac}E_{dc} + 2\delta_{3333}E_{ac}E_{dc}H_{dc})(V/\mu_o), \quad (17)$$

provides all relevant magnetoelectric (ME) coupling coefficients a_{ij}, β_{ijk}, γ_{ijk}, and δ_{ijkl} under suitable measurement strategies.

First of all, we have tested *linear* ME coupling by measuring m_{ME}' on the weakly dilute AF compound $CuCr_{0.8}In_{0.2}P_2S_6$ (see Fig. 15 and 16) at $T < T_N$ as a function of E_{ac} alone. The resulting data (not shown) turned out to oscillate around zero within errors, hence, $\alpha \approx 0$ ($\pm 10^{-12}$ s/m). This is disappointing, since the (average) monoclinic space group C2/m (Colombet et al., 1982) is expected to reveal the linear ME effect similarly as in $MnPS_3$ (Ressouche et al., 2010). We did, however, not yet explore non-diagonal couplings, which are probably more favorable than collinear field configurations.

More encouraging results were found in testing higher order ME coupling as found, *e. g.*, in the disordered multiferroics $Sr_{0.98}Mn_{0.02}TiO_3$ (Shvartsman et al., 2008) and $PbFe_{0.5}Nb_{0.5}O_3$ (Kleemann et al., 2010). Fig. 20 shows the magnetic moment m_{ME}' resulting from the weakly dilute AF compound $CuCr_{80}In_{20}P_2S_6$ after ME cooling to below T_N in three applied fields, E_{ac}, E_{dc}, and (a) at variant H_{dc} with constant $T = 10$ K, or (b) at variant T and constant $\mu_0H_{dc} = 2$ T.

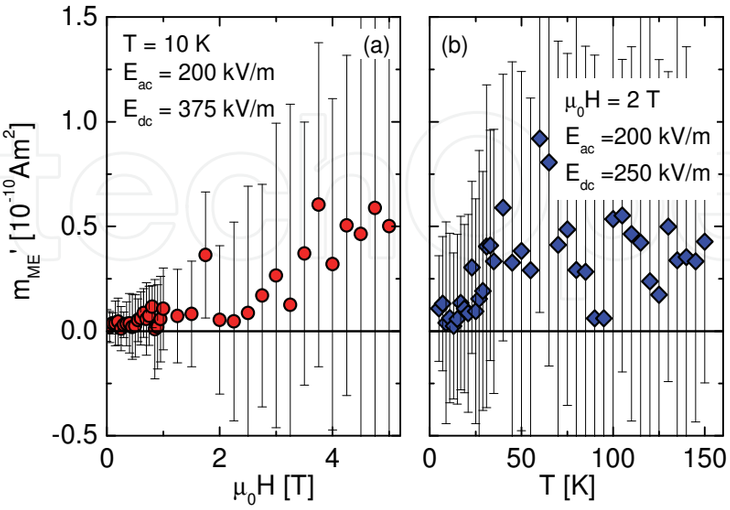

Fig. 20. Magnetoelectric moment m_{ME}' of $CuCr_{0.8}In_{0.2}P_2S_6$ excited by $E_{ac} = 200$ kV/m at $f = 1$ Hz in constant fields E_{dc} and H_{dc} and measured parallel to the c axis (a) *vs.* μ_0H at $T = 5$ K and (b) *vs.* T at $\mu_0H = 2$ T.

We notice that very small, but always positive signals appear, although their large error limits oscillate around $m_{ME}' = 0$. That is why we dismiss a finite value of the second-order magneto-bielectric coefficient γ_{333}, which should give rise to a finite ordinate intercept at $H = 0$ in Fig. 20a according to *Eq.* (17). However, the clear upward trend of $\langle m_{ME}' \rangle$ with increasing magnetic field makes us believe in a finite *biquadratic* coupling coefficient. The average slope in Fig. 20a suggests $\delta_{3333} = \mu_o \Delta m_{ME}' / (2V \Delta H_{dc} E_{ac} \Delta E_{dc}) \approx 4.4 \times 10^{-25}$ sm/VA. This value is more than one to two orders of magnitude smaller than those measured in $Sr_{0.98}Mn_{0.02}TiO_3$ (Shvartsman et al., 2008) and $PbFe_{0.5}Nb_{0.5}O_3$ (Kleemann et al., 2010), $\delta_{3333} \approx -9.0 \times 10^{-24}$ and 2.2×10^{-22} sm/VA, respectively. Even smaller, virtually vanishing values are found for the more dilute paramagnetic compounds such as $CuCr_{0.5}In_{0.5}P_2S_6$ (not shown). The temperature dependence of m_{ME}' in Fig. 20b shows an abrupt increase of noise above $T_N = 23$ K. This hints at disorder and loss of ME response in the paramagnetic phase.

3.6 Summary

The dilute antiferromagnets $CuCr_{1-x}In_xP_2S_6$ reflect the lamellar structure of the parent compositions in many respects. First, the distribution of the magnetic Cr^{3+} ions is dilute from the beginning because of their site sharing with Cu and (P_2) ions in the basal *ab* planes. This explains the relatively low Néel temperatures (< 30 K) and the rapid loss of magnetic percolation when diluting with In^{3+} ions ($x_c \approx 0.3$). Second, at $x > x_c$ the AF transition is destroyed and local clusters of exchange-coupled Cr^{3+} ions mirror the layered structure by their nearly compensated total moments. Deviations of the magnetization from Curie-Weiss behavior at low T and strong anisotropy remind of super-AF clusters with quasi-molecular magnetic properties. Third, only weak third order ME activity was observed, despite favorable symmetry conditions and occurrence of two kinds of ferroic ordering for $x < x_c$, ferrielectric at $T < 100$ K and AF at $T < 30$ K. Presumably inappropriate experimental conditions have been met and call for repetition. In particular, careful preparation of ME single domains by orthogonal field-cooling and measurements under non-diagonal coupling conditions should be pursued.

4. Piezoelectric and ultrasonic investigations of phase transitions in layered ferroelectrics of $CuInP_2S_6$ family

Ultrasonic investigations were performed by automatic computer controlled pulse-echo method and the main results are presented in papers (Samulionis et al., 2007; Samulionis et al., 2009a; Samulionis et al., 2009b). Usually in $CuInP_2S_6$ family crystals ultrasonic measurements were carried out using longitudinal mode in direction of polar c-axis across layers. The pulse-echo ultrasonic method allows investigating piezoelectric and ferroelectric properties of layered crystals (Samulionis et al., 2009a). This method can be used for the indication of ferroelectric phase transitions. The main feature of ultrasonic method is to detect piezoelectric signal by a thin plate of material under investigation. We present two examples of piezoelectric and ultrasonic behavior in the $CuInP_2S_6$ family crystals, viz. $Ag_{0.1}Cu_{0.9}InP_2S_6$ and the nonstoichiometric compound $CuIn_{1+\delta}P_2S_6$. The first crystal is interesting, because it shows tricritical behavior, the other is interesting for applications, because when changing the stoichiometry the phase transition temperature can be increased. For the layered crystal $Ag_{0.1}Cu_{0.9}InP_2S_6$, which is not far from pure $CuInP_2S_6$ in the phase diagram, we present the temperature dependence of the piezoelectric signal when

a short ultrasonic pulse of 10 MHz frequency is applied (Fig. 20). At room temperature no signal is detected, showing that the crystal is not piezoelectric. When cooling down a signal of 10 MHz is observed at about 285 K. It increases with decreasing temperature. Obviously piezoelectricity is emerging.

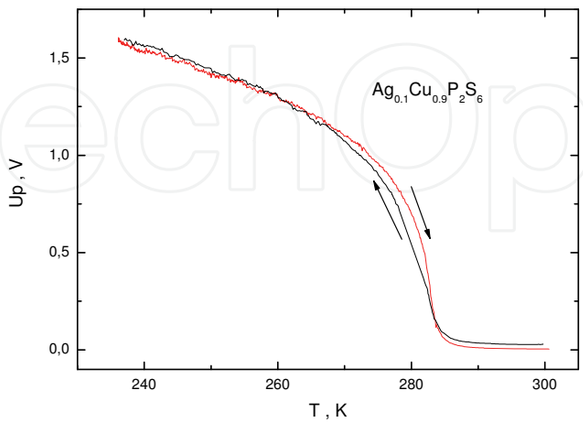

Fig. 21. Temperature dependences of ultrasonically detected piezoelectric signal in an $Ag_{0.1}Cu_{0.9}InP_2S_6$ crystal. Temperature variations are shown by arrows.

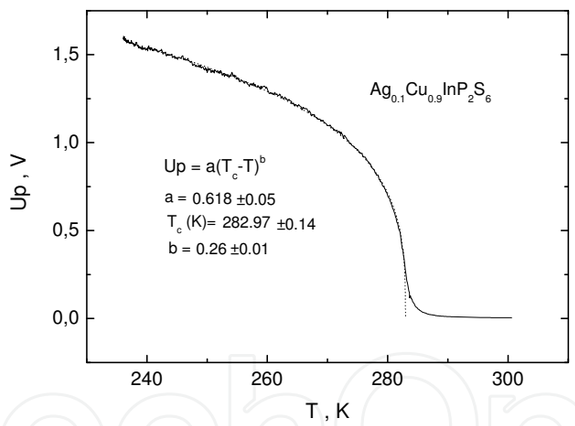

Fig. 22. Temperature dependences of the amplitude of piezoelectric signal and the least squares fit to *Eq.* (18), showing that the phase transition is close to the tricritical one.

The absence of temperature hysteresis shows that the phase transition near $T_c = 283$ K is close to second-order. In order to describe the temperature dependence of the amplitude of the ultrasonically detected signal we applied a least squares fit using the equation:

$$U_p = A(T_c - T)^{\beta} \tag{18}$$

In our case the piezoelectric coefficient g_{33} appears in the piezoelectric equations. The tensor relation of the piezoelectric coefficients implies that $\boldsymbol{g} = \mathbf{d}\ \boldsymbol{\varepsilon}_t^{-1}$. According to (Strukov & Levanyuk, 1995) the piezoelectric coefficient d in a piezoelectric crystal varies as $d \propto \eta_0/(T_c\text{-}T)$. Assuming that the dielectric permittivity $\boldsymbol{\varepsilon}_t$ can be approximated by a Curie

law it turns out that the amplitude of our ultrasonically detected signal varies with temperature in the same manner as the order parameter η_0. Hence, according to the fit in Fig. 22 the critical exponent of the order parameter (polarization) is close to the tricritical value of 0.25.

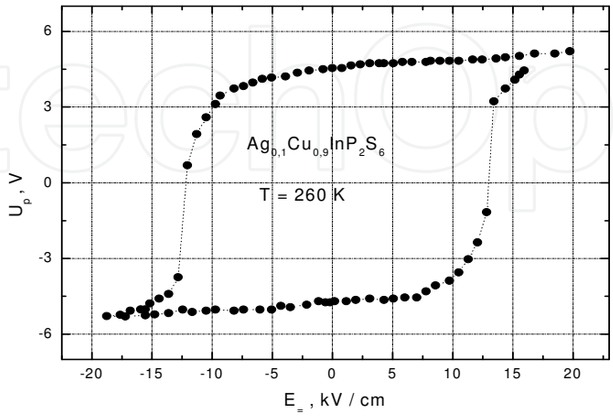

Fig. 23. dc field dependence of the piezoelectric signal amplitude in a $Ag_{0.1}Cu_{0.9}InP_2S_6$ crystal

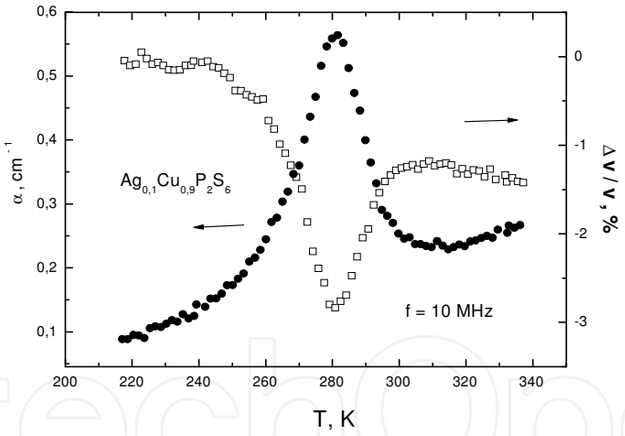

Fig. 24. Temperature dependences of the longitudinal ultrasonic attenuation and velocity in a $Ag_{0.1}Cu_{0.9}InP_2S_6$ crystal along the *c*-axis

In the low temperature phase hysteresis-like dependencies of the piezoelectric signal amplitude on dc electric field with a coercive field of about 12 kV/cm were obtained (Fig. 23). Thus the existence of the ferroelectric phase transition was established for $Ag_{0.1}Cu_{0.9}InP_2S_6$ crystal. The existence of the phase transition was confirmed by both ultrasonic attenuation and velocity measurements. Since the layered samples were thin, for reliable ultrasonic measurements the samples were prepared as stacks from 8-10 plates glued in such way that the longitudinal ultrasound can propagate across layers. At the phase transition clear ultrasonic anomalies were observed (Fig. 24). The anomalies were similar to those which were described in pure $CuInP_2S_6$ crystals and explained by the

interaction of the elastic wave with polarization (Valevicius et al., 1994a; Valevicius et al., 1994b). In this case the relaxation time increases upon approaching T_c according to Landau theory (Landau & Khalatnikov, 1954) and an ultrasonic attenuation peak with downwards velocity step can be observed. The increase of velocity in the ferroelectric phase can be attributed to the contribution of the fourth order term in the Landau free energy expansion. In this case the velocity changes are proportional to the squared order parameter. Also the influence of polarization fluctuations must be considered especially in the paraelectric phase.

Obviously the increase of the phase transition temperature is a desirable trend for applications. Therefore, it is interesting to compare the temperature dependences of ultrasonically detected electric signals arising in thin pure $CuInP_2S_6$, $Ag_{0.1}Cu_{0.9}InP_2S_6$ and indium rich $CuInP_2S_6$, where *c*-cut plates are employed as detecting ultrasonic transducers. Exciting 10 MHz lithium niobate transducers were attached to one end of a quartz buffer, while the plates under investigation were glued to other end. Fig. 24 shows the temperature dependences of ultrasonically detected piezoelectric signals in thin plates of these layered crystals. For better comparison the amplitudes of ultrasonically detected piezoelectric signals are shown in arbitrary units. It can be seen, that the phase transition temperatures strongly differ for these three crystals. The highest phase transition temperature was observed in nonstoichiometric $CuInP_2S_6$ crystals grown with slight addition of In i.e. $CuIn_{1+\delta}\ P_2S_6$ compound, where δ = 0.1 - 0.15. The phase transition temperature for an indium rich crystal is about 330 K. At this temperature also the critical ultrasonic attenuation and velocity anomalies were observed similar to those of pure $CuInP_2S$ crystals.

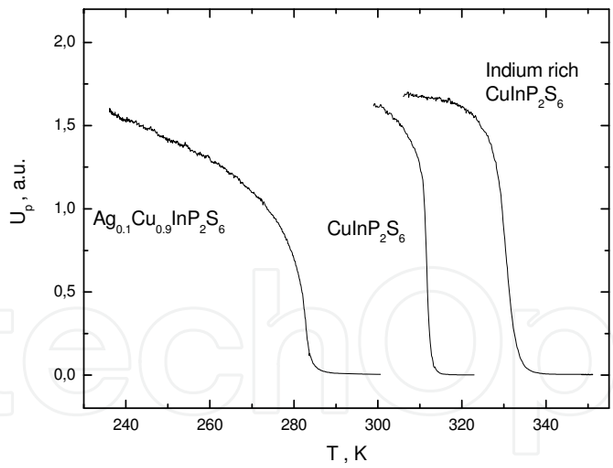

Fig. 25. The temperature dependences of ultrasonic signals detected by c-cut plates of $CuInP_2S_6$, $Ag_{0.1}Cu_{0.9}InP_2S_6$ and indium rich $CuInP_2S_6$ crystals.

Absence of piezoelectric signals above the phase transition shows that the paraelecric phases are centrosymetric. But at higher temperature piezoelectricity induced by an external *dc* field due to electrostriction was observed in $CuIn_{1+\delta}\ P_2S_6$ crystalline plates. In this case a large electromechanical coupling (K = 20 – 30 %) was observed in *dc* fields of order 30 kV/cm. It is necessary to note that the polarisation of the sample in a *dc* field in the field cooling regime strongly increases the piezosensitivity. In these $CuIn_{1+\delta}P_2S_6$ crystals at room temperature an

electromechanical coupling constant as high as > 50 % was obtained after appropriate poling, what is important for applications.

5. Conclusions

It was determined from dielectric permittivity measurements of layered $CuInP_2S_6$, $Ag_{0.1}Cu_{0.9}InP_2S_6$ and $CuIn_{1+\delta}P_2S_6$ crystals in a wide frequency range (20 Hz to 3 GHz) that:

1. A first-order phase transition of order – disorder type is observed in a $CuInP_2S_6$ crystal doped with Ag (10%) or In (10%) at the temperatures 330 K and 285 K respectively. The type of phase transition is the same as in pure $CuInP_2S_6$ crystal.
2. The frequency dependence of dielectric permittivity at low temperatures is similar to that of a dipole glass phase. Coexistence of ferroelectric and dipole glass phases or of nonergodic relaxor and dipole glass phase can be observed because of the disorder in the copper sublattice created by dopants.

Low frequency (20 Hz – 1 MHz) and temperature (25 K and 300 K) dielectric permittivity measurements of $CuCrP_2S_6$ and $CuIn_{0.1}Cr_{0.9}P_2S_6$ crystals have shown that:

1. The phase transition temperature shifts to lower temperatures doping $CuCrP_2S_6$ with 10 % of indium and the phase transition type is of first-order as in pure $CuCrP_2S_6$.

Layered $CuIn_xCr_{1-x}P_2S_6$ mixed crystals have been studied by measuring the complex dielectric permittivity along the polar axis at frequencies 10^{-5} Hz - 3 GHz and temperatures 25 K – 350 K Dielectric studies of mixed layered $CuIn_xCr_{1-x}P_2S_6$ crystals with competing ferroelectric and antiferroelectric interaction reveal the following results:

1. A dipole glass state is observed in the intermediate concentration range $0.4 \le x \le 0.5$ and ferroelectric or antiferroelectric phase transition disappear.
2. Long range ferroelectric order coexists with the glassy state at $0.7 \le x \le 1$.
3. A phase transition into the antiferroelectric phase occurs at $0 \le x \le 0.1$, but here no glass-like relaxation behavior is observed.
4. The distribution functions of relaxation times of the mixed crystals calculated from the experimental dielectric spectra at different temperatures have been fitted with the asymmetric double potential well model. We calculated the local polarization distributions and temperature dependence of macroscopic polarization and Edwards – Anderson order parameter, which shows a second-order phase transition.

Solid solutions of $CuCr_{1-x}In_xP_2S_6$ reveal interesting magnetic properties, which are strongly related to their layered crystal structure:

1. Diamagnetic dilution with In^{3+} of the antiferromagnetic $x = 0$ compound experiences a low percolation threshold, $x_p \approx 0.3$, toward 'superparamagnetic' disorder without tendencies of blocking or forming spin glass.
2. At low temperatures the 'superparamagnetic' clusters in $x > 0.3$ compounds reveal strong magnetic anisotropy, which suggests them to behave like 'molecular magnets'.

Crystals of the layered $CuInP_2S_6$ family have large piezoelectric sensitivity in their low temperature phases. They can be used as ultrasonic transducers for medical diagnostic applications, because the PT temperature for indium rich $CuInP_2S_6$ crystals can be elevated up to 330 K.

6. Acknowledgment

Thanks are due to P. Borisov, University of Liverpool, for help with the magnetic and magneto-electric measurements.

7. References

Banys, J., Klimm, C., Völkel, G., Bauch, H. & Klöpperpieper, A. (1994). Proton-glass behavior in a solid solution of (betaine phosphate)0.15 (betaine phosphite)0.85, *Phys. Rev. B*., Vol. 50, p. 16751 – 16753

Banys, J., Lapinskas, S., Kajokas, A., Matulis, A., Klimm, C., Völkel, G. & Klöpperpieper, A. (2002). Dynamic dielectric susceptibility of the betaine phosphate (0.15) betaine phosphite (0.85) dipolar glass *Phys. Rev. B*, Vol. 66, pp. 144113

Banys, J., Macutkevic, J., Samulionis, V., Brilingas, A. & Vysochanskii, Yu. (2004). Dielectric and ultrasonic investigation in $CuInP_2S_6$ crystals, *Phase Transitions*, Vol. 77, pp. 345 - 358

Bertrand, D., Bensamka, F., Fert, A. R., Gélard, F., Redoulès, J. P. & Legrand, S. (1984). Phase diagram and high-temperature behaviour in dilute system $Fe_xMg_{1-x}Cl_2$, J. *Phys. C: Solid State Phys*., Vol. 17, pp. 1725 – 1734

Bertrand, D., Fert, A. R., Schmidt, M. C., Bensamka, F. & Legrand, S. (1982). Observation of a spin glass-like behaviour in dilute system $Fe_{1-x}Mg_xCl_2$, *J. Phys. C: Solid State Phys*., Vol. 15, pp. L883 – L888

Blundell, S. (2001). *Magnetism in Condensed Matter* (1st edition), Oxford Univ. Press, ISBN 019850591, Oxford

Blundell, S. (2007). Molecular magnets, *Contemp. Phys*., Vol. 48, pp. 275 - 290

Bogani, L. & Wernsdörfer, W. (2008). Molecular spintronics using single-molecule magnets, *Nat. Mater*., Vol. 7, pp. 179 – 186

Borisov, P., Hochstrat, A., Shvartsman, V.V. & Kleemann, W. (2007). Superconducting quantum interference device setup for magnetoelectric measurements, *Rev. Sci. Instrum*. Vol. 78, pp. 106105-1 -106105-3

Cajipe, V. B., Ravez, J., Maisonneuve, V,. Simon, A., Payen, C., Von Der Muhll, R. & Fischer, J. E. (1996). Copper ordering in lamellar $CuMP_2S_6$ (M = Cr, In): transition to an antiferroelectric or ferroelectric phase, *Ferroelectrics* 185, pp.135 - 138

Carlin, R.L. (1984). In: *Magneto-structural correlations in exchange-coupled systems*, *NATO ASI Series,* Willett, R.D., Gatteschi, D., Kahn, O. (Eds.),Vol. 140, pp. 127-155. Reidel, ISBN: 978-90-277-1876-1, Dordrecht

Colombet, P., Leblanc, A., Danot, M. & Rouxel, J. (1982). Structural aspects and magnetic properties of the lamellar compound $Cu_{0.50}Cr_{0.50}P_2S_6$, *J. Sol. State Chem.* Vol. 41, 174

Dziaugys, A., Banys, J., Macutkevic, J., Sobiestianskas, R., Vysochanskii, Yu. (2010). Dipolar glass phase in ferrielectrics: $CuInP_2S_6$ and $Ag_{0.1}Cu_{0.9}InP_2S_6$ crystals, *Phys. Stat. Sol. (a)*, Vol. 8, pp. 1960 - 1967

Dziaugys, A., Banys, J. & Vysochanskii, Y. (2011). Broadband dielectric investigations of indium rich $CuInP_2S_6$ layered crystals, *Z. Kristallogr*., Vol. 226, pp.171-176.

Gatteschi, D., Sessoli, R. & Villain, J. (2006). *Molecular Nanomagnets,* Oxford University Press, ISBN 0198567537, Oxford

Goossens, D. J., Struder, A. J., Kennedy, S. J. & Hicks, T. J. (2000). The impact of magnetic dilution on magnetic order in $MnPS_3$, *Phys.: Condens. Matter*, Vol. 12, pp. 4233 - 4242

Grigas, J. (1996). *Microwave dielectric spectroscopy of ferroelectrics and related materials*, Gordon & Breach Science Publishers, Amsterdam

Kim, B., Kim, J. & Jang, H. (2000). Relaxation time distribution of deuterated dipole glass, *Ferroelectrics,* Vol. 240, pp. 249

Kittel, C. (1951), Theory of antiferroelectric crystals, *Phys. Rev.* Vol. 82, pp. 729-732

Kleemann, W., Bedanta, S., Borisov, P., Shvartsman, V. V., Miga, S., Dec, J., Tkach, A. & Vilarinho, P. M. (2009). Multiglass order and magnetoelectricity in Mn^{2+} doped incipient ferroelectrics, *Eur. Phys. J. B*, Vol. 71, pp. 407 - 410

Kleemann, W., Shvartsman, V. V., Borisov, P. & Kania, A. (2010). Coexistence of antiferromagnetic and spin cluster glass order in the magnetoelectric relaxor multiferroic $PbFe_{0.5}Nb_{0.5}O_3$, *Phys. Rev. Lett.*, Vol. 105, pp. 257202-1 -257202-4

Klingen, W., Eulenberger, G. & Hahn, H. (1973). Über die Kristallstrukturen von FeP_2Se_6 und $Fe_2P_2S_6$, *Z. Anorg. Allg. Chem.*, Vol. 401, pp. 97 - 112

Landau, L. & Khalatnikov, I., (1954). About anomalous sound attenuation near the phase transition of second-order (in Russian), *Sov. Phys. (Doklady)*, Vol. 96, pp. 459- 466

Macutkevic, J., Banys, J., Grigalaitis, R. & Vysochanskii, Y. (2008). Asymmetric phase diagram of mixed $CuInP_2(S_xSe_{1-x})_6$ crystals, *Phys.Rev. B*, Vol. 78, pp. 06410-1 - 06410-3

Maior, M. M., Motria, S. F., Gurzan, M. I., Pritz, I. P. & Vysochanskii, Yu. M. (2008). Dipole glassy state in layered mixed crystals of $Cu(In,Cr)P_2(S,Se)_6$ system, *Ferroelectrics*, Vol. 376, pp. 9 - 16

Maisonneuve, V., Evain, M., Payen, C., Cajipe, V. B. & Molinie, P. (1995). Room-temperature crystal structure of the layered phase $Cu^{I}In^{III}P_2S_6$, *J. Alloys Compd.*, Vol. 218, pp.157-164

Maisonneuve, V., Cajipe, V. B., Simon, A., Von Der Muhll, R. & Ravez, J. (1997). Ferrielectric ordering in lamellar $CuInP_2S_6$, *Phys. Rev. B*, Vol. 56, pp. 10860 - 10868

Mattsson, J., Kushauer, J., Bertrand, D., Ferré, J., Meyer, P., Pommier, J. & Kleemann, W. (1996). Phase diagram and mixed phase dynamics of the dilute Ising antiferromagnet $Fe_{1-x}Mg_xCl_2$, $0.7 \leq x < 1$. *J. Magn. Magn. Mat.*, Vol. 152, pp. 129 - 138

Mulders, A. M., Klaasse, J. C. P. , Goossens, D. J., Chadwick, J. & Hicks, T. J. (2002). High-field magnetization in the diluted quasi-two-dimensional Heisenberg antiferromagnet $Mn_{1-x}Zn_xPS_3$, *J. Phys.: Condens. Matter*, Vol. 14, pp. 8697

Mydosh, J. A. (1993). Spin glasses - an experimental introduction (first edition), Taylor & Francis, ISBN 0748400389, Oxford

Néel, L. (1961). Superparamagnétisme des grains très fins antiferromagnétiques, *Acad. Sci. Paris, C. R.*, Vol. 252, 4075 – 4080

Pelster, R., Kruse, T., Krauthäuser, H.G., Nimtz, G. & Pissis P. (1998). Analysis of 2-Dimensional Energy and Relaxation Time Distributions from Temperature-Dependent Broadband Dielectric Spectroscopy, *Phys. Rev. B*, Vol. 57, pp. 8763 - 8766

Ressouche, E., Loire, M., Simonet, V., Ballou, R., Stunault, A. & Wildes, A. (2010). Magnetoelectric $MnPS_3$ as a candidate for ferrotoroidicity, *Phys. Rev. B,* Vol. 82, pp. 100408(R)-1 - 100408(R)-4

Samulionis, V., Banys, J. & Vysochanskii, Y. (2009a). Piezoelectric and elastic properties of layered materials of $Cu(In,Cr)P_2(S,Se)_6$ system, *J. Electroceram.*, Vol. 22, pp. 192-197

Samulionis, V., Banys, J. & Vysochanskii, Y. (2009b). Linear and nonlinear elastic properties of $CuInP_2S_6$ layered crystals under polarization reversal, *Ferroelectrics*, Vol. 379, pp. 293-300

Samulionis, V., Banys, J. & Vysochanskii, Y. (2007). Piezoelectric and Ultrasonic Studies of Mixed $CuInP_2(S_XSe_{1-X})_6$ Layered Crystals *Ferroelectrics*, Vol. 351, pp. 88-95

Schafer, H., Sternin, H. E., Stannarius, R., Arndt, M. & Kremer, F. (1996), Novel Approach to the Analysis of Broadband Dielectric Spectra, *Phys. Rev. Lett.*, Vol. 76, pp. 2177-2180.

Shvartsman, V. V., Bedanta, S., Borisov, P., Kleemann, W., Tkach, A. & Vilarinho, P. M. (2008). (Sr,Mn)TiO_3 - a magnetoelectric multiglass, *Phys. Rev. Lett*., Vol. 101, pp. 165704-1 - 165704-4

Simon, A., Ravez, J., Maisonneuve, V., Payen, C. & Cajipe, V. B. (1994). Paraelectric-ferroelectric transition in the lamellar thiophosphate $CuInP_2S_6$. *Chem. Mater.*, Vol. 6, pp. 1575 - 1580

Strukov, B. A. & Levanyuk, A. (1995). *Ferroelectric phenomena in crystals* (in Russian*),* Nauka-Fizmatlit*,* Moscow, p.117.

Valevicius, V., Samulionis, V. & Banys, J. (1994). Ultrasonic dispersion in the phase transition region of ferroelectric materials, *J. Alloys Compd.*, Vol. 211/212, pp. 369-373

Valevicius, V., Samulionis, V., Banys, J., Grigas, J. & Yagi, T. (1994). Ultrasonic study of ferroelectric phase transition in DDSP, *Ferroelectrics*, Vol. 156, pp. 365-370

Vysochanskii, Yu. M., Stepanovich, V. A., Molnar, A. A., Cajipe, V. B. & Bourdon, X. (1998). Raman spectroscopy study of the ferrielectric-paraelectric transition in layered $CuInP_2S_6$*, Phys. Rev. B*., Vol. 58, pp. 9119 - 9124

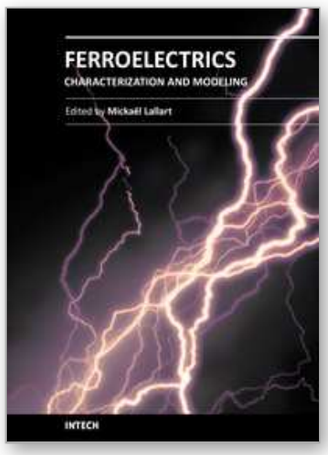

Ferroelectrics - Characterization and Modeling

Edited by Dr. MickaÃ«l Lallart

ISBN 978-953-307-455-9
Hard cover, 586 pages
Publisher InTech
Published online 23, August, 2011
Published in print edition August, 2011

Ferroelectric materials have been and still are widely used in many applications, that have moved from sonar towards breakthrough technologies such as memories or optical devices. This book is a part of a four volume collection (covering material aspects, physical effects, characterization and modeling, and applications) and focuses on the characterization of ferroelectric materials, including structural, electrical and multiphysic aspects, as well as innovative techniques for modeling and predicting the performance of these devices using phenomenological approaches and nonlinear methods. Hence, the aim of this book is to provide an up-to-date review of recent scientific findings and recent advances in the field of ferroelectric system characterization and modeling, allowing a deep understanding of ferroelectricity.

InTech Europe
University Campus STeP Ri
Slavka Krautzeka 83/A
51000 Rijeka, Croatia
Phone: +385 (51) 770 447
Fax: +385 (51) 686 166
www.intechopen.com

InTech China
Unit 405, Office Block, Hotel Equatorial Shanghai
No.65, Yan An Road (West), Shanghai, 200040, China
中国上海市延安西路65号上海国际贵都大饭店办公楼405单元
Phone: +86-21-62489820
Fax: +86-21-62489821

IntechOpen